

Magnetic shielding property for cylinder with circular, square, and equilateral triangle holes

Si-Yuan Hao(郝思源), Xiao-Ping Lou(娄小平), Jing Zhu(祝静), Guang-Wei Chen(陈广伟), and Hui-Yu Li(李慧宇)
Citation: Chin. Phys. B, 2021, 30 (**6**): 060702. DOI: 10.1088/1674-1056/abeeee
Journal homepage: http://cpb.iphy.ac.cn; http://iopscience.iop.org/cpb

What follows is a list of articles you may be interested in

A modified analytical model of the alkali-metal atomic magnetometer employing longitudinal carrier field

Chang Chen(陈畅), Yi Zhang(张燚), Zhi-Guo Wang(汪之国), Qi-Yuan Jiang(江奇渊), Hui Luo(罗晖), and Kai-Yong Yang(杨开勇)
Chin. Phys. B, 2021, 30 (**5**): 050707. DOI: 10.1088/1674-1056/abd7d3

Search for topological defect of axionlike model with cesium atomic comagnetometer

Yucheng Yang(杨雨成), Teng Wu(吴腾), Jianwei Zhang(张建玮), and Hong Guo(郭弘)
Chin. Phys. B, 2021, 30 (**5**): 050704. DOI: 10.1088/1674-1056/abf132

Atomic magnetometer with microfabricated vapor cells based on coherent population trapping

Xiaojie Li(李晓杰), Yue Shi(史越), Hongbo Xue(薛洪波), Yong Ruan(阮勇), and Yanying Feng(冯焱颖)
Chin. Phys. B, 2021, 30 (**3**): 030701. DOI: 10.1088/1674-1056/abc2b9

A synthetic optically pumped gradiometer for magnetocardiography measurements

Shu-Lin Zhang(张树林), Ning Cao(曹宁)
Chin. Phys. B, 2020, 29 (**4**): 040702. DOI: 10.1088/1674-1056/ab7801

Standing-wave spectrometry in silicon nano-waveguides using reflection-based near-field scanning optical microscopy

Yi-Zhi Sun(孙一之), Wei Ding(丁伟), Bin-Bin Wang(王斌斌), Rafael Salas-Montiel, Sylvain Blaize, Renaud Bachelot, Zhong-Wei Fan(樊仲维), Li-Shuang Feng(冯丽爽)
Chin. Phys. B, 2019, 28 (**1**): 010702. DOI: 10.1088/1674-1056/28/1/010702

Magnetic shielding property for cylinder with circular, square, and equilateral triangle holes*

Si-Yuan Hao(郝思源)[1,2,3], Xiao-Ping Lou(娄小平)[1,2,3,†], Jing Zhu(祝静)[1,2,3], Guang-Wei Chen(陈广伟)[1,2,3], and Hui-Yu Li(李慧宇)[1,2,3]

[1] *Key Laboratory of the Ministry of Education for Optoelectronic Measurement Technology and Instrument, Beijing* 100192, *China*
[2] *Beijing Laboratory of Optical Fiber Sensing and System, Beijing Information Science & Technology University, Beijing* 100016, *China*
[3] *Beijing Key Laboratory of Optoelectronic Measurement Technology, Beijing Information Science & Technology University, Beijing* 100192, *China*

(Received 18 December 2020; revised manuscript received 18 February 2021; accepted manuscript online 16 March 2021)

The shielding property of cylinder with circular, square, and equilateral triangle holes was investigated by finite element analysis (FEA). The hole area ($S_{\rm hole}$) plays an important role in magnetic circuit on the surface of cylinder. When $S_{\rm hole}$ is less than the critical area ($S_{\rm H}$), cylinder with three shapes of holes obtained the same remanent magnetization inside, indicating that the shielding property is unaffected by the shape of the hole. Hence, high-permeability material is the major path of the magnetic field. On the condition of $S_{\rm hole} > S_{\rm H}$, the sequence of the shielding property is equilateral triangle > square > circular, resulting from magnetoresistance of leakage flux in air dielectric. Besides, the anisotropy of shielding property caused by hole structural differences of the cylinder is evaluated. We find that a good shielding effectiveness is gained in the radial direction, compared with the axis direction. This research focuses on providing a theoretical support for the design of magnetic shield and improvement on the magnetic shielding ability.

Keywords: SERF atomic magnetometer, magnetic shielding, holes, finite element analysis (FEA)

PACS: 07.55.Ge, 41.20.Gz, 07.05.Tp **DOI:** 10.1088/1674-1056/abeeee

1. Introduction

High sensitivity magnetometry techniques have gained more attention in many fields of basic research and applications, such as physics, biology, neuroscience, materials science, and geology.[1,2] The common magnetic sensors include fluxgate magnetometer, proton precession magnetometer, superconducting quantum interference devices (SQUIDs), and optically atomic magnetometers (OPAMs) working in the spin-exchange relaxation free (SERF) regime.[3]

SQUIDs and SERF magnetometer are two of the most sensitive magnetic sensors used in weak magnetic field detection. SQUIDs are demonstrated an ultrahigh sensitivity of 1 fT/Hz$^{1/2}$,[4] but operate in a low temperature environment causing high maintenance charge and manufacturing costs. Compared with SQUIDs, the sensitivity of SERF magnetometer has reached 0.16 fT/Hz$^{1/2}$ in the low-frequency range.[5] Due to the advantages of low power consumption, non-cryogenic operation and high spatial resolution, SERF magnetometer has become one of the most potential weak magnetic field detection devices.[6] However, all the weak magnetic measurements based on SERF magnetometer are performed in magnetically shielded rooms for providing a nearly zero magnetic field circumstance.[7] The sensitivity of SERF magnetometer theoretically is 0.01 fT/Hz$^{1/2}$, and the ambient magnetic field noise is the key factor limiting the augment of sensitivity in laboratory (0.16 fT/Hz$^{-1/2}$).[8] Thus, high-performance magnetic shielding system plays an important role in suppressing the ambient magnetic field noise and increasing ultrahigh sensitive magnetic measurement.

Compared with air, high magnetic permeability (μ) materials with small magnetic resistance, provide magnetic circuit for the Earth's magnetic field, resulting in high-performance magnetic shield inside. Cylinder is one of the most widely used structures, with advantages of simple manufacture and high shielding performance.[9,10] Hole located on the surface of shielding cylinder is necessary to keep light and wire of equipment passing through, resulting in more leakage fluxes and less shielding ability. Therefore, shielding property depended on hole structure is an important problem, which was studied by many scholars. Ma *et al.*[11] explored the effect on shield ratio when holes and gaps exist, simultaneously. They quantitatively analyzed magnetic shielding ratio for a range of hole diameters and gap thicknesses in the transverse and longitudinal direction, using the finite element method. Besides, the relationship between shielding factor of a spherical shell and the diameter of hole was reported by Xuan *et al.*[12]

In this paper, the relationship between shielding property and the shape of hole structure was investigated by finite element analysis (FEA). There are circular, square, and equilateral triangle shapes. In addition, the anisotropy of shielding

*Project supported by the Key Projects of the National Natural Science Foundation of China (Grant No. 51535002) and the Programme of Introducing Talents of Discipline to Universities (Grant No. D17021).

†Corresponding author. E-mail: louxiaoping@bistu.edu.cn

© 2021 Chinese Physical Society and IOP Publishing Ltd

property was evaluated by analyzing the residual field on the X, Y, and Z directions, individually.

2. Shielding principle and simulation method

Shielding factors (S) and shielding effectiveness (SE) are used to assess the magnetic shielding performance of cylinder.[13] The definitions are given as follows:

$$S = \frac{B_o}{B_i}, \tag{1}$$

$$SE = 20\log\left(\frac{B_o}{B_i}\right), \tag{2}$$

where B_i and B_o are the magnetic fields in the same position with and without magnetic shield, respectively.

Material and structure are two key factors for improving shielding performance of cylinder.[14] On the one hand, the Earth's magnetic field is one of the typical static magnetic fields. Magnetic shielding cylinder is made of ferromagnetic material with high permeability. The permeability of a ferromagnetic material is several thousand times greater than that of air, and, the reluctance of a cavity is much greater than that of a ferromagnetic material. Therefore, the vast majority of the external magnetic induction lines will pass along the walls of the ferromagnetic material, and entering the cavity with very little fluxes.

On the other hand, multi-layer shielding cylinder is used to screen out the residual magnetic flux leaking into the cavity again and again to achieve better shielding effectiveness. Structure parameters include innermost layer radius (R) and length (L), single layer thickness (T), radial gap (ΔR) and axial gap (ΔL) between layers, and number of layer (n). The axial shielding factor is proportional to n, μ, T, ΔR and inversely proportional to R, L, and ΔL.[15] The model of axial shielding factor was optimized by nonlinear programming quadratic line (NLPQL) algorithm, and a combination of optimum parameters was obtained.[16]

Because of the economic efficiency and the experimental error, FEA method was selected to simulate the Earth's magnetic field and establish the three-dimensional model of shielding cylinder. The diagrams of the external and internal structures of the shielding cylinder are shown in Figs. 1(a)–1(b), which is made up of the curving tube body and the planar cover. In this research, structure parameters of shield on the basis of Ref. [16] are shown in Table 1, and R, L, ΔR, ΔL, T, and n are equal to 11.0 cm, 33.0 cm, 1.6 cm, 2.0 cm, 0.2 cm, and 5.0, respectively. Permalloy material is selected and its relative permeability is approximately equal to 2×10^4. The three-dimensional model of shielding cylinder with square, circular, and equilateral triangle holes are established and illustrated in Figs. 1(c)–1(e), separately. Because, the small vacuum vapor of the SERF magnetometer is located at center position of the shield, two holes are designed and placed at the center of cover and body, separately.

Table 1. Parameters of the magnetic shielding cylinder.

Parameter	Value
R (cm)	11
L (cm)	33
ΔR (cm)	1.6
ΔL (cm)	2
T (cm)	0.2
n	5

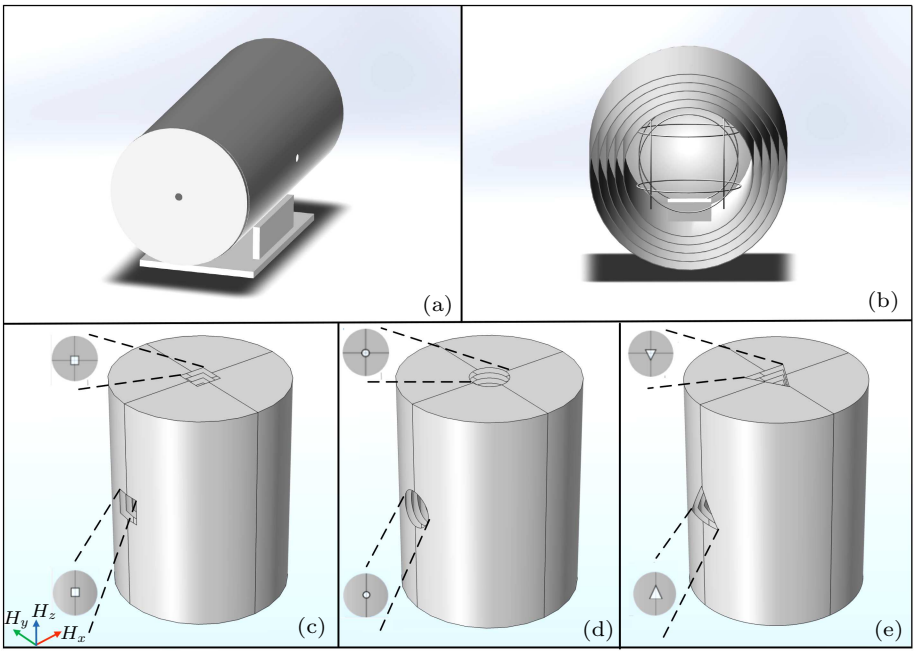


Fig. 1. (a) External and (b) internal structures of the cylinder. The three-dimensional model of the shielding cylinder with square (c), circular (d), and equilateral triangle (e) holes.

Due to the structural anisotropy of shielding cylinder, there are significant differences about shielding properties between axis (Z direction) and radial direction (X direction and Y direction). The SE of radial direction is much more than that of axial direction.[17] Regarded as a uniformly distributed field, the geomagnetic field intensity vector is approximately equal to 50.0 μT. H_X, H_Y, and H_Z represent the orthogonal decomposition of the magnetic field vector on the X, Y, and Z axes. Based on the superposition theorem, H_X, H_Y, and H_Z are set as 26.7 μT in this paper to assess the shielding property in different directions, individually.

3. Results and discussion

The magnetic field in center position of cylinder is named "the central magnetic field (M)", which is used to evaluate the shielding property of cylinder with various shape holes. The size of hole area (projected area) is an important factor in magnetic field transmission on the surface of cylinder.[18] The relationship of hole area (S_{hole}), M, and hole shapes in X, Y, and Z directions is simulated and illustrated as shown in Fig. 2. M_{C}, M_{S}, and M_{ET} are the M contributed by cylinders with circular, square, and equilateral triangle holes, respectively.

The values of S_{hole} range from 0 to 150 cm^2, and are limited by R equaling to 156.32 cm^2. With the increase of S_{hole}, the values of M_{C}, M_{S}, and M_{ET} increase with various rates. S_{max} is defined as the maximum of S_{hole} on condition of low speed. When S_{hole} is less than S_{max}, M_{C}, M_{S}, and M_{ET} rise slowly as shown in the inset of Figs. 2(a)–2(c). The growth rate increases rapidly when S_{hole} is greater than S_{max}. Therefore, S_{max} is the optimum hole area, which is marked in the inset of Fig. 2. The S_{max} in X, Y, and Z directions are equal to 2.56, 23.00, 7.29 cm^2, and M_{C}, M_{S}, and M_{ET} are equivalent to 1.953×10^{-2} nT, 1.505×10^{-2} nT, and 0.809 nT, respectively. Thus, S and SE in X, Y, and Z directions are equal to 1.367×10^6 and 122.715, 1.774×10^6, and 124.986, and 3.302×10^5 and 110.370 at $S_{\text{hole}} = S_{\text{max}}$, separately.

The effect of various hole shapes on shielding property is limited by S_{hole}. The critical area (S_{H}) in X, Y, and Z directions are equal to 8.41, 23.00, 14.44 cm^2 respectively, as shown in Figs. 2(a)–2(c). When S_{hole} is less than S_{H}, the cylinder with three shapes of holes obtains the same remanent magnetization inside, indicating that the shielding property is unaffected by the shape of the hole. On the condition of $S_{\text{hole}} > S_{\text{H}}$, M_{C}, M_{S}, and M_{ET} increase in an order of $M_{\text{C}} > M_{\text{S}} > M_{\text{ET}}$, indicating that the types of the hole shape have obvious effect on the shielding property.

In addition, the anisotropy of the shielding property is evaluated by analyzing the residual fields on the X, Y, and Z directions, individually. As is shown in Figs. 1(c)–1(e), H_Z is perpendicular to the hole in cover of cylinder but horizontal to the hole in body. The relationship between H_X and hole in tube body and cover is contrary compared with H_Z. H_Y is horizontal to the two holes designed in this paper. $(\theta_{\text{cover}}, \theta_{\text{body}})_X$, $(\theta_{\text{cover}}, \theta_{\text{body}})_Y$, and $(\theta_{\text{cover}}, \theta_{\text{body}})_Z$ represent the θ between the magnetic field in the X, Y, and Z directions and holes in cylinder cover and body, and are equal to $(0°, 90°)_X$, $(0°, 0°)_Y$, and $(90°, 0°)_Z$. The values of M in X (M_X), Y (M_Y), and Z (M_Z) direction is in an order of $M_Z > M_X > M_Y$ under the same S_{hole} value and hole shape condition, as demonstrated in Fig. 2. Therefore, cylinder with various hole structures shows good shielding for Y-direction magnetic field because H_Y is horizontal to the two position holes.

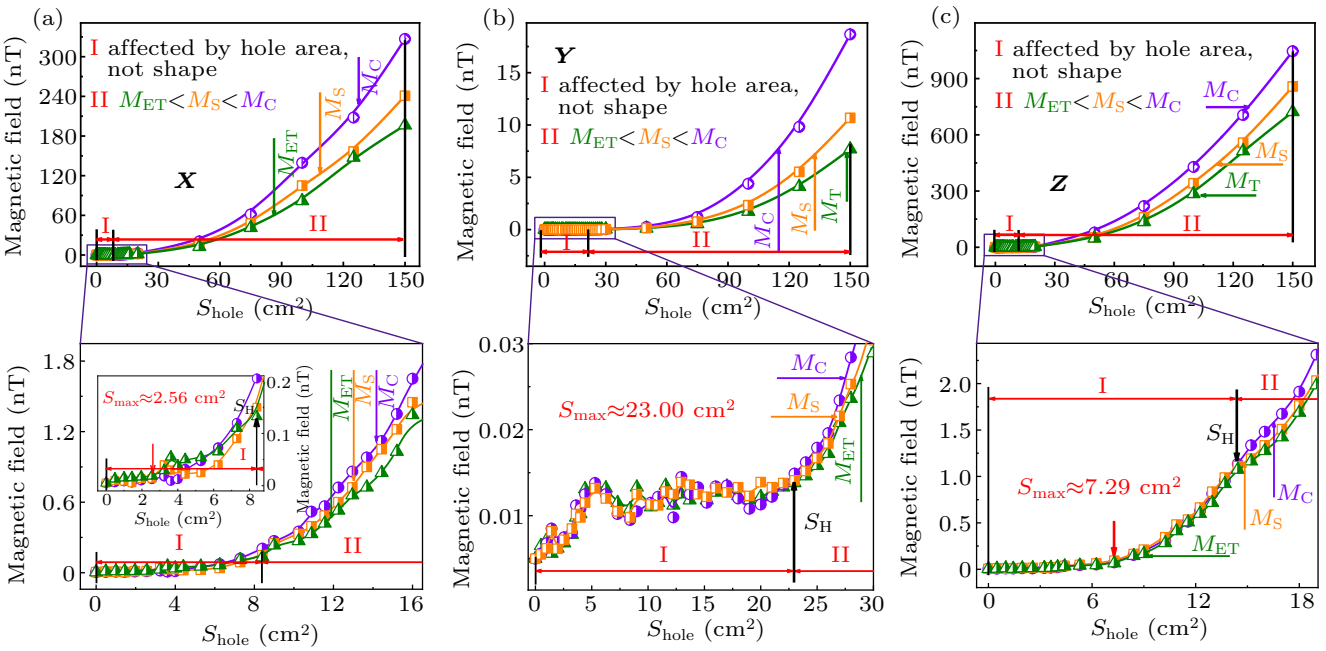


Fig. 2. The relationship between hole area, hole shapes, and M in X (a), Y (b), and Z (c) directions.

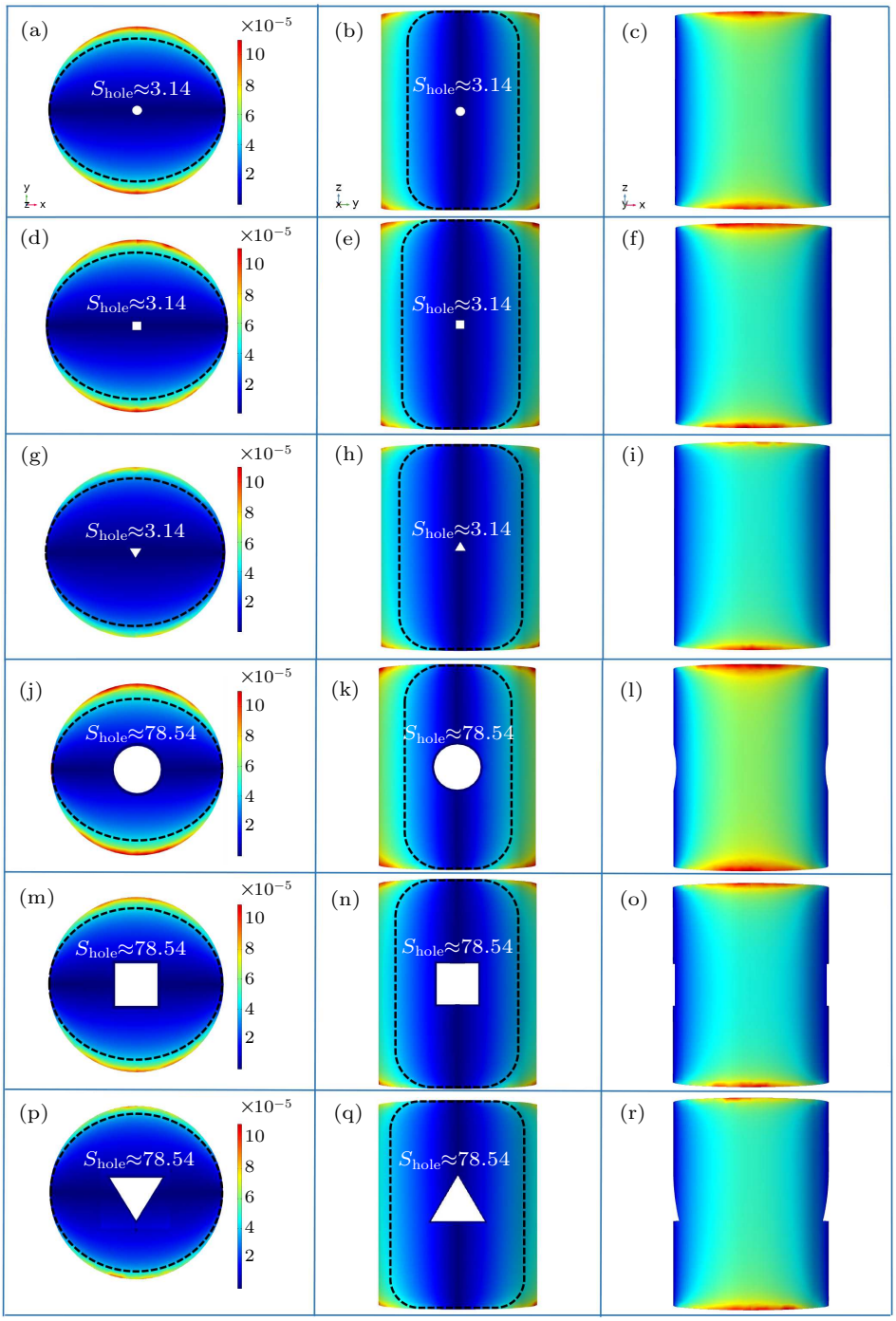


Fig. 3. The magnetic field distribution at Z, X, and Y axes of cylinder with circular, square, and equilateral triangle hole shapes on the condition of $S_{\text{hole}} \approx 3.14$ cm^2 [(a)–(i)] and $S_{\text{hole}} \approx 78.54$ cm^2 [(j)–(r)].

The right-angle structure in axial direction does not guide flux well, resulting in more magnetic flux leakings into the shielded region, worsening the shielding effectiveness.[19] Compared with the planar cover, there is a better shielding effectiveness of curving tube body, resulting in bigger M_Z than M_X. The axial shielding factor of cylinder is always smaller than the radial shielding factor.[20] The shielding property of cylinder was optimized by finite element analysis. The radial shielding factor was 20.6 times of the axial shielding factor.[21] Therefore, there is better shielding effectiveness in the radial direction, compared with axis direction, under the same hole shape and size condition.

Figure 3 shows the magnetic field distribution for cylinder with different hole shapes on the condition of $S_{\text{hole}} \approx 3.14$ cm^2 ($< S_{\text{H}}$) and $S_{\text{hole}} \approx 78.54$ cm^2 ($> S_{\text{H}}$). S_{Refrence} is defined as the area where the magnetic field value is less than or equal to 1.326 nT, marked by the black dotted line. Under the same magnetic field circumstance, the value of S_{Refrence} is bigger, the shielding capability is better. The S_{C}, S_{S}, and S_{ET} represent S_{Refrence} in cylinder with circular, square, and regular triangle holes. On the condition of $S_{\text{hole}} \approx 3.14$ cm^2, the hole shapes have little impact on the magnetic field distribution on

the surface of cylinder, resulting in $S_C = S_S = S_{ET}$, as demonstrated in Figs. 3(a)–3(i). By contrast, under the circumstance of $S_{hole} \approx 78.54$ cm^2, there is the same relationship among S_C, S_S, and S_{ET} in cylinder cover and body, that is $S_C < S_S < S_{ET}$, as exhibited in Figs. 3(j)–3(r). Thus, the sequence of the shielding ability of cylinder with various holes is equilateral triangle > square > circular.

The sketch of M dependence on S_{hole} is shown in Fig. 4. The purple, orange, and green curves represent M_C, M_S, and M_{ET} as a function of S_{hole}, respectively. Magnetostatic shielding obtained by shunting the magnetic flux and diverting it away from a shielded region. Compared with air, high-permeability material shows low magnetoresistance. It is realized by the introduction of ferromagnetic materials with high magnetic permeability, which creates a preferential path for the magnetic field lines. Higher leakage flux is the reason of that M_C, M_S, and M_{ET} augments with S_{hole} increasing.[22] The relationship between M and S_{hole} is in accordance with the result reported by Li *et al.*[23] In addition, on the condition of $S_{hole} < S_H$, various hole shapes have no effect on the shielding ability. Thus, high-permeability material is the major magnetic path. Under the condition of $S_{hole} > S_H$, the sequence of M is equilateral triangle < square < circular, indicating that the order of the shielding ability is circular < square < equilateral triangle. With the increase of S_{hole}, there are more leakage fluxes shown in air, and shielded pass through air and high-permeability material.

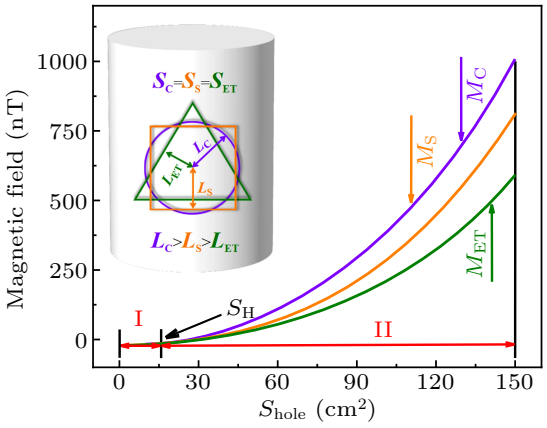


Fig. 4. The sketch of M_C, M_S, and M_{ET} dependence on S_{hole}.

Magnetoresistance (Z_m), the resistance of a magnetic path, is determined by the formula[24]

$$Z_m = F/\Phi, \tag{3}$$

where F and Φ are the magnetomotive force and magnetic flux. Under the condition of a uniform magnetic circuit, Φ is written as

$$\Phi = \mu \times H \times S, \tag{4}$$

where μ, H, and S are the permeability of material, magnetic intensity, and cross-sectional area, respectively. Z_m is written as

$$Z_m = \frac{F}{\mu \times H \times S} = \frac{L}{\mu S}, \tag{5}$$

where L is the length of magnetic circuit.

Z_C, Z_S, and Z_{ET} represent magnetoresistances of cylinder with circular, square, and equilateral triangle hole, separately. L_C, L_S, and L_{ET} represent the shortest lengths of the magnetic circuit of circular, square, and regular triangle holes, respectively. The mechanism of the model is proposed and exhibited as illustrated in Fig. 4. The order of L_C, L_S, and L_{ET} is $L_{ET} < L_S < L_C$, as shown in Fig. 4. On the same condition of cross-sectional area (S) and magnetic permeability (μ), the relationship between Z_C, Z_S, and Z_{ET} is $Z_C < Z_S < Z_{ET}$, resulting in $M_C > M_S > M_{ET}$. Thus, the order of the shielding property is circular < square < regular triangle. There is the most excellent shielding property of cylinder with equilateral triangle hole structure.

4. Conclusion and perspectives

In summary, based on FEA method, the effect of hole shapes on shielding effectiveness of cylinder was investigated in this research. The selected shapes are square, circular, and equilateral triangle. Because of the structural anisotropy of cylinder, M dependence on S_{hole} in Z, Y, and X directions was explored, and there is better shielding effectiveness in the radial direction, compared with the axis direction.

In addition, with the increase of S_{hole}, there are more leakage fluxes, resulting in augments M_C, M_S, and M_{ET}. However, when S_{hole} exceeds S_H, the sequence of the shielding ability is equilateral triangle > square > circular, due to the magnetoresistance of the leakage flux in air dielectric. The relationship between Z_C, Z_S, and Z_{ET} is $Z_C < Z_S < Z_{ET}$, resulting in $M_C > M_S > M_{ET}$. Therefore, there is the most excellent shielding property of cylinder with equilateral triangle hole structure.

Finally, the growth rate of M_C, M_S, and M_{ET} is different at various S_{hole}. When S_{hole} is less than S_{max}, M_C, M_S, and M_{ET} rise slowly. On the condition of $S_{hole} > S_{max}$, the growth rate increases rapidly. Therefore, S_{max} is identified as the optimum hole area.

References

[1] Colombo A P, Carter T R, Borna A, Jau Y Y, Johnson C N, Dagel A L and Schwindt D P 2016 *Opt. Express* **24** 15403
[2] Patton B, Zhivun E, Hovde D C and Budker D 2014 *Phys. Rev. Lett.* **113** 013001
[3] Li J J, Du P C, Fu J Q, Wang X T, Zhou Q and Wang R Q 2019 *Chin. Phys. B* **28** 040703
[4] Li J D, Quan W, Zhou B Q, Wang Z and Fang J C 2018 *IEEE Sens. J.* **18** 8198

[5] Dang H B, Maloof A C and Romalis M V 2010 *Appl. Phys. Lett.* **97** 151110
[6] Wyllie R, Kauer M, Smetana G S, Wakai R T and Walker T G 2012 *Phys. Med. Bio.* **57** 2619
[7] Canova A, Freschi F, Giaccone L and Repetto M 2017 *IEEE Trans. Magn.* **54** 1
[8] Kominis I, Kornack T W, Allred J C and Romalis M V 2003 *Nature* **422** 596
[9] Bai W X, Li T L, Guo A Q, Cheng R Q and Jiao C Q 2019 *Acta Phys. Sin.* **68** 104101 (in Chinese)
[10] Fu J Q, Du P C, Zhou Q and Wang R Q 2015 *Chin. Phys. B* **25** 010302
[11] Ma D Y, Ding M, Lu J X, Yao H, Zhao J P, Yang K, Cai J S and Han B C 2019 *IEEE Sens. J.* **19** 6085
[12] Xuan L, Dong H and Zhuo C 2013 *The 8th Annual IEEE International Conference on Nano/Micro Engineered and Molecular Systems*, April 7–10, 2013, Suzhou, China, p. 649
[13] Kornack T W, Smullin S J, Lee S K and Romalis M V 2007 *Appl. Phys. Lett.* **90** 223501
[14] Gubser D U, Wolf S A and Cox J E 1979 *Rev. Sci. Instrum.* **50** 751
[15] Li J D, Han B C, Liu F, Xing L and Liu G 2019 *IEEE Sens. J.* **19** 2916
[16] Donley E A, Hodby E, Hollberg L and Kitching J 2007 *Rev. Sci. Instrum.* **78** 083102
[17] Sumner T J, Pendlebury J M and Smith K F 1987 *J. Appl. Phys.* **20** 1095
[18] Paperno E, Romalis M V and Noam Y 2004 *IEEE Trans. Magn.* **40** 2170
[19] Wu J C, Li L, Harrison J C and Candler R N 2017 *19th International Conference on Solid-State Sensors, Actuators and Microsystems (TRANSDUCERS)*, June 18–22, 2017, Kaohsiung, Taiwan, China p. 838
[20] Donley E A, Hodby E, Hollberg L and Kitching J 2007 *Rev. Sci. Instrum.* **78** 083102
[21] Li J D, Quan W, Han B C, Wang Z and Fang J C 2019 *IEEE Sens. J.* **20** 1793
[22] Moric I, Laurent P, Chatard P, Graeve D C M, Thomin S, Christophe V and Grosjean O 2014 *Acta Astronaut.* **102** 287
[23] Li Q M, Zhang J H, Huang Z J, Zeng X J and Sun W M 2012 *Proceedings of* 2012 *International Conference on Measurement, Information and Control*, May 18–20, 2012, Harbin, China, p. 67
[24] Popov G M 2003 *Meas Technol.* **46** 377